CHEMISTRY
A EUROPEAN JOURNAL

DOI: 10.1002/chem.200701997

The Importance of the Long Type 1 Copper-Binding Loop of Nitrite Reductase for Structure and Function

Katsuko Sato, Susan J. Firbank, Chan Li, Mark J. Banfield, and Christopher Dennison*[a]

Abstract: The long 15-residue type 1 copper-binding loop of nitrite reductase has been replaced with that from the cupredoxin amicyanin (7 residues). This sizable loop contraction does not have a significant effect on the spectroscopy, and therefore, the structures of both the type 1 and type 2 Cu^{II} sites. The crystal structure of this variant with Zn^{II} at both the type 1 and type 2 sites has been determined. The coordination geometry of the type 2 site is almost identical to that found in the wild-type protein. However, the structure of the type 1 centre changes significantly upon metal substitution, which is an unusual feature for this class of site. The positions of most of the coordinating residues are altered of which the largest difference was observed for the coordinating His residue in the centre of the mutated loop. This ligand moves away from the active site, which results in a more open metal centre with a coordinating water molecule. Flexibility has been introduced into this region of the protein. The 200 mV increase in the reduction potential of the type 1 copper site indicates that structural changes upon reduction must stabilise the cuprous form. The resulting unfavourable driving force for electron transfer between the two copper sites, and an increased reorganisation energy for the type 1 centre, contribute to the loop variant having very little nitrite reductase activity. The extended type 1 copper-binding loop of this enzyme makes a number of interactions that are important for maintaining quaternary structure.

Keywords: copper · cupredoxin · electron transfer · loop-directed mutagenesis · nitrite reductase

Introduction

Copper-containing nitrite reductases (NIRs) catalyse a key step in denitrification, which is part of the global nitrogen cycle.[1] NIRs are usually trimeric with each subunit consisting of two β-barrel domains, with that towards the N-terminus possessing a mononuclear electron transferring type 1 (T1) copper site.[2–8] The copper ion is bound by three strong equatorial ligands that are provided by the thiolate sulfur of a Cys residue and the imidazole nitrogen atoms of two His residues. An axially interacting Met residue approximately 2.5 Å from the metal completes the distorted tetrahedral geometry. The catalytic type 2 (T2) copper centre is coordinated in an almost perfect tetrahedral arrangement between two subunits of the WT NIR trimer by three His residues and a water ligand. Nitrite binds at this T2 site and is reduced to nitric oxide with an electron provided by a redox metalloprotein via the T1 copper site (the T1 and T2 copper centres are 12.5 Å apart).[1,9] An unusual structural feature of NIR is the extended 15-residue C-terminal T1 copper-binding loop, on which the Cys, one of the His and the Met ligands are situated. The corresponding region in other proteins usually consists of only seven to eleven residues.[7,10–12]

Loop-directed mutagenesis has been used to analyse the effect of swapping T1 copper-binding loops in a range of single-domain, β-barrel, electron-transfer (ET) proteins (cupredoxins).[10–21] In particular, the shortest naturally occurring loop of amicyanin (AMI; seven residues) has been successfully introduced into plastocyanin (PC) and pseudoazurin (PAZ), both of which have nine-residue loops, and azurin (AZ), which has a ten-residue loop.[16,17] The structures of the AZAMI[19] and PAZAMI[21] chimeras demonstrate that the introduced loops adopt a conformation as in AMI. The AZAMI variant has a reduction potential (E_m) value that is almost identical to that of AMI, which highlights that loop conformation tunes this important property.[17,19,20] In

[a] Dr. K. Sato, Dr. S. J. Firbank, Dr. C. Li, Dr. M. J. Banfield, Dr. C. Dennison
Institute for Cell and Molecular Biosciences
Medical School, Newcastle University
Newcastle upon Tyne
NE2 4HH (UK)
Fax: (+44) 191-222-7424
E-mail: christopher.dennison@ncl.ac.uk

Supporting information for this article is available on the WWW under http://www.chemeurj.org/ or from the author.

PAZAMI, interactions between the introduced loop and the PAZ scaffold result in active-site alterations that also influence E_m.[21] The structure of the PAZAMI T1 copper site changes very little upon redox interconversion,[21] which is recognised as an important feature of this family of proteins because it minimises the reorganisation energy and allows fast ET.[22–24] The rigid cupredoxin fold is thought to be important in this respect, but theoretical studies have suggested that the ligand set and geometry (provided by the protein) are almost equally acceptable for both Cu^{II} and Cu^{I}.[25]

The unique extended T1 copper-binding loop of NIR contributes to packing within the subunits and also to monomer–monomer interactions. We have, therefore, chosen NIR as the most suitable model for assessing additional roles, as well as binding a functional T1 copper site, of the metal-binding loop of a cupredoxin domain within a multi-copper enzyme. The very short AMI loop has been introduced into NIR and a detailed characterisation performed, which included crystal-structure determination of this chimera. Loop contraction in NIR does not prevent T1 copper binding, but renders the enzyme almost totally inactive.

Results

Purification and characterisation of NIRAMI: The NIRAMI variant elutes from a cation exchange column as two blue fractions, with visible absorbance maxima (λ_{max}) at 600 nm ($NIRAMI_{600}$) and 610 nm ($NIRAMI_{610}$), which are characteristic of T1 S(Cys)→Cu^{II} ligand-to-metal charge-transfer (LMCT) bands. These two fractions do not separate further on an anion exchange column, however, on a gel filtration column, $NIRAMI_{600}$ and $NIRAMI_{610}$ both elute as a mixture of trimer and monomer. The two forms of $NIRAMI_{600}$ and the $NIRAMI_{610}$ monomer have λ_{max} values of 600 nm for their main LMCT band, whereas the $NIRAMI_{610}$ trimer has a λ_{max} value of 610 nm. For $NIRAMI_{610}$, the trimeric form predominates, with relatively small amounts of monomer present. The actual quantity of monomer present varied between different preparations, but was usually $<10\,\%$, thus the mixture has a λ_{max} value of 610 nm. For $NIRAMI_{600}$, the relative amounts of trimer and monomer varied, with usually slightly more trimer present. When the trimeric and monomeric forms of $NIRAMI_{600}$ were reapplied to the Superdex 75 column, both eluted as a mixture of trimer and monomer. It was, therefore, considered appropriate to study $NIRAMI_{600}$ as a mixture of monomer and trimer, whereas studies with $NIRAMI_{610}$ were performed with purified trimer. MALDI-TOF mass spectrometry analysis of NIRAMI gave a mass of $M_r = 35\,892$ compared with the calculated value of $M_r = 35\,886.9$ (which includes the N-terminal Met residue introduced when cloning the wild-type (WT) NIR gene.

The UV/Vis spectra of Cu^{II}–$NIRAMI_{600}$ and $NIRAMI_{610}$ are compared in Figure 1a and those of $NIRAMI_{610}$, WT NIR and AMI from *Paracoccus versutus* are shown in Figure 1b (band positions and molar absorption coefficient (ε) values are listed in Table 1). The ε values at λ_{max} for the two different forms of NIRAMI are shown as being identical, but the copper concentration was only determined for $NIRAMI_{600}$. The EPR spectrum of $NIRAMI_{600}$ has a single Cu^{II} signal that can be readily assigned to the T1 copper site (see Figure 2), and therefore, this form of the variant has very little T2 or adventitious copper that could interfere with this analysis. The $A_{280}/A_{\approx 600}$ ratios for $NIRAMI_{600}$ and $NIRAMI_{610}$ are similar, which indicates that the $\varepsilon_{\approx 600}$ values are alike. The $NIRAMI_{600}$ sample used in the EPR studies was a mixture of trimeric and monomeric forms, and therefore, neither of these was able to bind a T2 copper site (see Figure 2). All attempts to reconstitute the T2 site of $NIRAMI_{600}$ with Cu^{II} were unsuccessful. The T2 copper EPR signal for $NIRAMI_{610}$ is similar to that for the WT protein (see Figure 2a, parameters are listed in Table 1). The T1 EPR signals for $NIRAMI_{600}$ and $NIRAMI_{610}$ are alike (see Figure 2a and Table 1) and are only slightly different to that of WT NIR (see Figure 2b, parameters are listed in Table 1). A notable difference is that g_z increases while A_z decreases in NIRAMI compared with WT NIR, which gives values more like those found in this region of the AMI spectrum.

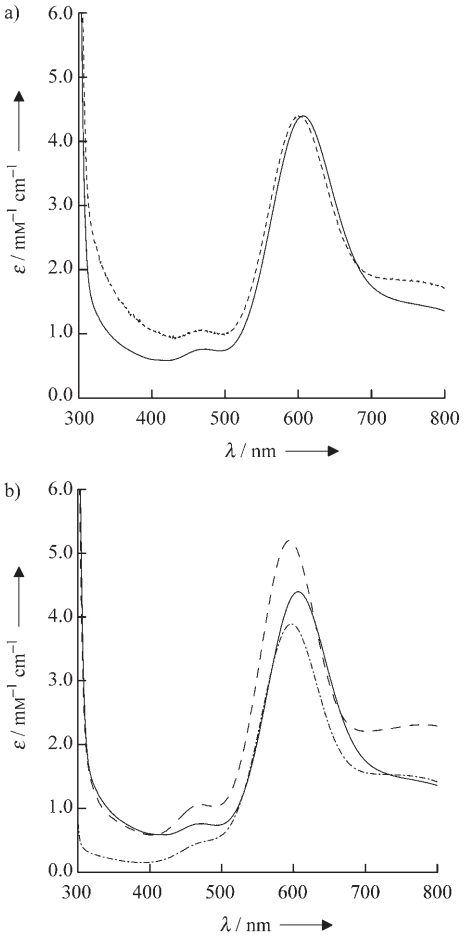

Figure 1. UV/Vis spectra ($T = 25\,°C$) of a) $NIRAMI_{600}$ (-----) and $NIRAMI_{610}$ (——) and b) $NIRAMI_{610}$ (——), WT NIR (– – –), and AMI from *P. versutus* (–•–•).

Table 1. T1 and T2 copper site properties of NIRAMI, WT NIR, and AMI.

	$NIRAMI_{610}$	$NIRAMI_{600}$	WT NIR	AMI[a]
UV/Vis[b]				
λ_1 [nm]	≈470	≈470	≈470	≈460
ε [$M^{-1}cm^{-1}$]	–	1060	1040	470
λ_2 [nm]	610	600	594	596
ε [$M^{-1}cm^{-1}$]	–	4400	5200	3900
$A_{\approx460}/A_{\approx600}$	0.17	0.24	0.20	0.11
EPR (T1 Cu)[c]				
g_x	≈2.04	2.043	2.042	2.032
g_y	≈2.04	2.043	2.042	2.047
g_z	≈2.24	2.228	2.215	2.235
A_x [mT]	≈1	0.9	1.1	0.6
A_y [mT]	≈1	0.9	0.9	0.8
A_z [mT]	≈5	5.8	6.3	5.4
EPR (T2 Cu)[d]				
g_z	2.35	–	2.32	–
A_z [mT]	12.5	–	13.5	–
E_m [mV][e]	–[f]	460[g]	260[h]	255[i]

[a] Data for AMI from *P. versutus*. [b] Conditions: $T=25\,°C$; $NIRAMI_{610}$ and $NIRAMI_{600}$: 20 mM phosphate (pH 7.0); WT NIR: 20 mM Mes (pH 6.0); AMI: 10 mM phosphate (pH 8.0). The molar absorption coefficient (ε) value for $NIRAMI_{600}$ at λ_2 is probably similar to that for $NIRAMI_{610}$, given that they have almost identical $A_{280}/A_{\approx600}$ ratios. [c] Conditions: $T=-196\,°C$; $NIRAMI_{610}$: 20 mM Tris (pH 7.5); $NIRAMI_{600}$: 25 mM Hepes (pH 8.6); WT NIR: 15 mM Mes (pH 6.0) 130 mM NaCl, 20% glycerol; and AMI: 25 mM Hepes (pH 7.6) and 40% glycerol. The T1 Cu site simulation for $NIRAMI_{610}$ was performed on the spectrum of a sample that also contained T2 copper, and thus the parameters obtained are less precise. [d] Values obtained directly from line positions. [e] Reduction potentials were measured at $(23\pm1)\,°C$ by cyclic voltammetry and values are quoted against the normal hydrogen electrode. [f] An electrochemical response could not be obtained for $NIRAMI_{610}$. [g] Determined in 20 mM Tris (pH 7.5; ionic strength = 0.10 M, NaCl). [h] Value taken from ref. [26]. [i] Value taken from ref. [27].

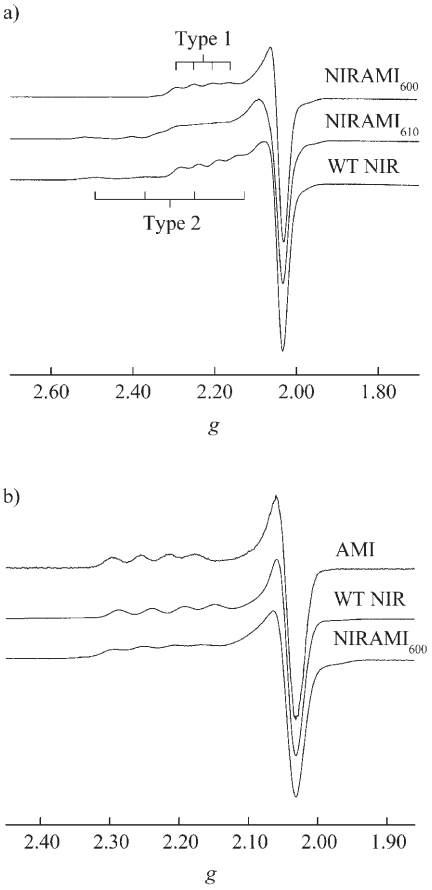

Figure 2. EPR spectra ($T=-196\,°C$) of a) $NIRAMI_{600}$, $NIRAMI_{610}$, and T2 copper-loaded WT NIR and b) $NIRAMI_{600}$, T2 copper-depleted WT NIR, and AMI from *P. versutus*.

The E_m value of $NIRAMI_{600}$ was determined by direct protein electrochemistry. The responses obtained on a modified gold electrode are less than ideal: the anodic and cathodic peaks have unequal intensities. Peak separations are around 120 mV at a scan rate of 3 $mV\,s^{-1}$ and this increases at faster scan rates; this indicates slow ET between the enzyme and the electrode, which has been reported previously for the WT protein.[26] Peak currents are proportional to the (scan rate)$^{1/2}$ in the range 3 to 50 $mV\,s^{-1}$. The E_m values at pH 6.5 and 7.5 are approximately 460 mV and approximately 440 mV at pH 8.5; these values are about 200 mV higher than that reported for the T1 copper site of the WT NIR (260 mV in 100 mM phosphate buffer at pH 7).[26] The relative catalytic activities of NIR and $NIRAMI_{610}$ (which exists mainly as a trimer and is the only form of the NIRAMI variant that binds a T2 copper site) have been assessed by using an assay in which reduced methyl viologen (MV) acts as the electron donor.[28,29] These studies indicate that the loop variant has very little activity, which is highlighted by the observation that the absorbance changes over the time period of the assay (typically 10 min.) were too small in experiments with NIRAMI to be precisely measured, except at high nitrite concentrations.

Overall structures of WT NIR and NIRAMI: Both WT NIR and NIRAMI crystallise in space group *H*3 with similar unit cell dimensions. This crystal form has previously been reported for *Alcaligenes xylosoxidans* NIR variants[30] and has been observed for the WT protein.[70] An atomic-resolution structure for WT NIR is available (1OE1)[4] and the root-mean-square deviation (RMSD) for the 335 equivalent C^α atoms between the WT NIR structure reported herein and 1OE1 is 0.25 Å. We have, therefore, used the 1OE1 structure for all subsequent comparisons. Crystallisation of NIRAMI was only achieved with the $NIRAMI_{610}$ form in the presence of 5 mM Zn^{II} (WT NIR crystallised in the presence of 10 mM Zn^{II}), despite numerous attempts with a wide range of conditions using different forms of the variant (see the Experimental Section). NIRAMI and WT NIR crystallise as trimers in identical oligomeric arrangements (a monomer in the asymmetric unit with the trimer generated by rotational crystallographic symmetry). The contact/buried water-accessible surface area between the subunits is similar in NIRAMI (2173 $Å^2$) and NIR (2199 $Å^2$), as are the hydro-

phobicity, planarity and the number of hydrogen bonds at this interface.

The overall structure of NIRAMI is very similar to that of WT NIR,[4] with 323 equivalent C^{α} atoms that superimpose with an RMSD of 0.38 Å (Figure 3a). The most significant alteration is in the ligand-containing loop, which has been mutated from C^{130}APEGMVPW-H^{139}VVSGM^{144} in WT NIR to C^{130}TPH^{133}PFM^{136} in NIRAMI. The backbone of the Cys-to-Met loop in NIRAMI is remarkably similar to that found in AMI from *Paracoccus denitrificans* (protein data bank (PDB) code 1AAC),[31] with an RMSD of 0.77 Å for the C^{α} atoms (see Figure 3b). The greatest C^{α} displacements between the loops of NIRAMI and AMI are observed for residues Thr131 and Pro134 (NIRAMI numbering) at 1.17 and 1.09 Å, respectively. These changes result from differing interactions between the loop and the WT NIR and AMI scaffolds (see the Supporting Information). The introduction of the short AMI sequence removes the α-helical section of the WT NIR loop (see Figure 3a), which is at the subunit interface and is involved in a number of important interactions within a single subunit. In WT NIR, the side chains of residues in this region make important monomer–monomer contacts that are missing in NIRAMI (see the Supporting Information). The number of hydrogen bonds around the active site of NIRAMI is dramatically reduced compared with WT NIR and matches that found for AMI (see Table S1 and description in the Supporting Information).[31]

Metal-site structures: The structures of the T1 and T2 copper sites in *A. xylosoxidans* WT NIR, determined herein, are essentially identical to those in the high-resolution structure reported previously (see Figure 3c and Tables 2 and 3).[4] In the case of the NIRAMI variant, which crystallised over a long period from a condition containing 5 mM Zn^{II}, completely colourless crystals, presumably with Zn^{II} present at

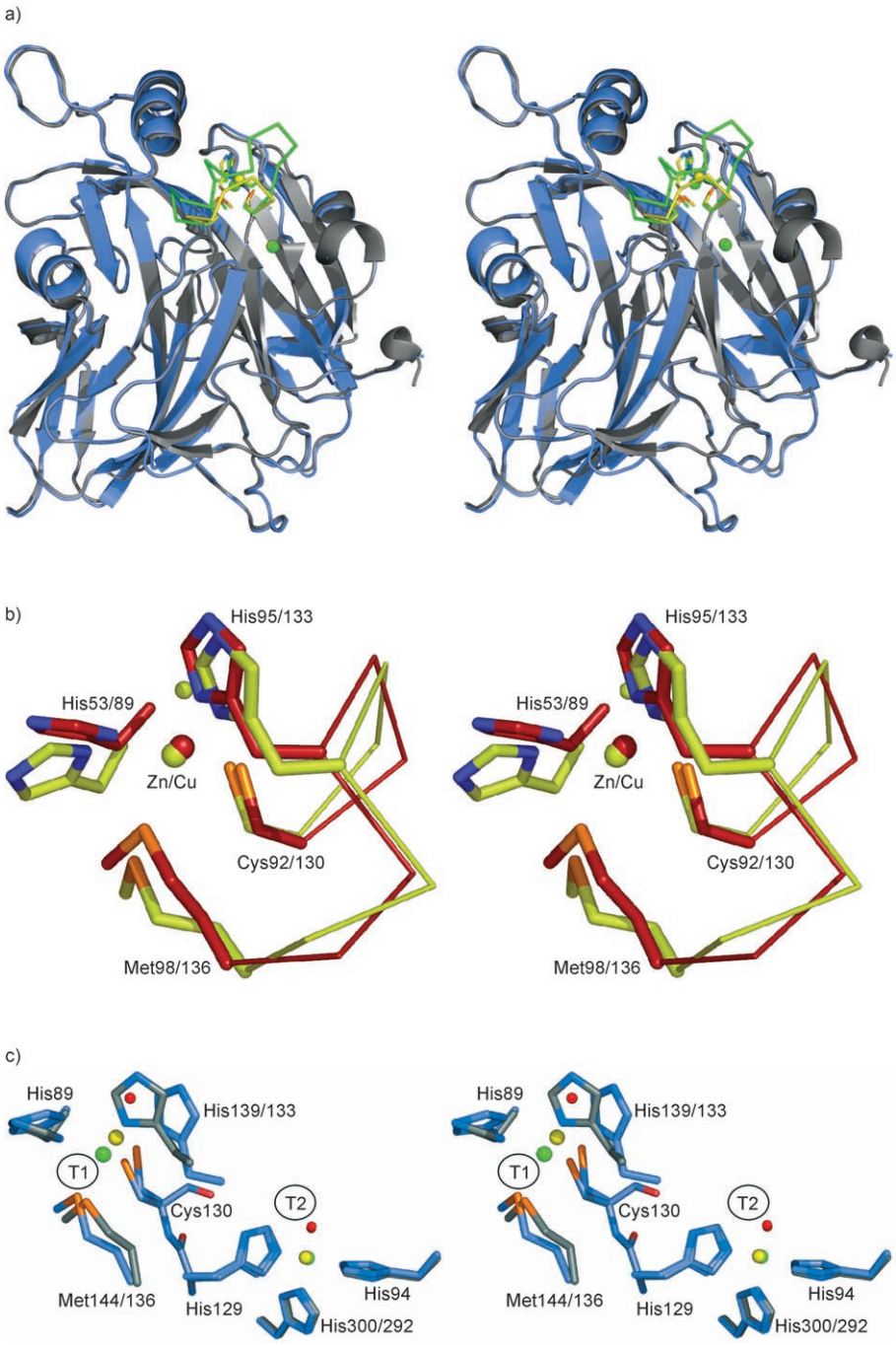

Figure 3. a) A stereoview of an overlay of the structures of WT NIR (PDB 1OE1, grey) and NIRAMI (blue). The ligand-containing loop, coordinating residues and metal ions at the T1 and T2 sites are coloured green in WT NIR and yellow in NIRAMI. b) A stereoview of an overlay of the T1 sites of AMI from *P. denitrificans* (1AAC, red) and NIRAMI (yellow). The ligating side chains are labelled according to their positions in AMI and NIRAMI, respectively. ●: Cu^{II} ion of AMI, ●: Zn^{II} ion of NIRAMI, ●: coordinating water in NIRAMI. c) A stereoview of an overlay of the active sites of WT NIR (ligands: grey, Cu^{II}: ●) and NIRAMI (ligands: blue, Zn^{II}: ●). The ligating side chains are labelled according to their positions in WT NIR and NIRAMI, respectively. ●: coordinated water at the T2 site (both proteins) and the T1 site (NIRAMI only).

Table 2. The geometry of the T1 metal sites of NIRAMI, WT NIR, and AMI.

	Zn^{II}–NIRAMI	Cu^{II}–WT NIR[a]	Cu^{II}–WT NIR (1OE1)[b]	Cu^{II}–AMI[c]
M–ligand bond lengths [Å]				
M–O(Pro88)	4.18	4.12	4.12	3.92
M–$N^{\delta1}$(His89)	2.57	2.23	2.02	1.95
M–S^{γ}(Cys130)	2.19	2.19	2.20	2.11
M–$N^{\delta1}$(His133)	2.37	2.00	2.03	2.03
M–S^{δ}(Met136)	3.55	2.54	2.45	2.90
M–O(H_2O)[d]	2.01	–	–	–
NSN plane[e]	0.14	0.56	0.60	0.30
angles [°]				
H_2O-M-His89	92	–	–	–
H_2O-M-Cys130	89	–	–	–
H_2O-M-His133	79	–	–	–
H_2O-M-Met136	162	–	–	–
His89-M-Cys130	117	124	122	136
His89-M-His133	132	99	101	104
His89-M-Met136	70	87	88	85
Cys130-M-His133	110	116	113	113
Cys130-M-Met136	98	113	114	111
His133-M-Met136	114	114	116	100

[a] Distances from the structure of *A. xylosoxidans* WT NIR (determined herein), in which His139 and Met144 replace His133 and Met136, respectively. [b] Obtained from the high-resolution structure of *A. xylosoxidans* WT NIR. [c] Obtained from the structure of *P. denitrificans* AMI (PDB code 1AAC), in which Pro52, His53, Cys92, His95, and Met98 replace Pro88, His89, Cys130, His133, and Met136, respectively. [d] This water molecule coordinates to Zn^{II} in the NIRAMI structure only. [e] The plane that contains His89, Cys130, and His136 ligands in NIRAMI.

Table 3. The geometry of the T2 sites of NIRAMI and WT NIR.

	Zn^{II}–NIRAMI	Cu^{II}–WT NIR[a]	Cu^{II}–WT NIR (1OE1)[b]
M–ligand bond lengths [Å]			
M–O(H_2O)	1.95	1.83	1.98
M–$N^{\varepsilon2}$(His94)	2.15	2.12	1.96
M–$N^{\varepsilon2}$(His129)	2.09	1.97	2.00
M–$N^{\varepsilon2}$(His292)	2.16	2.15	2.00
$O^{\delta2}$(Asp92)–H_2O	2.66	2.71	2.54
angles [°]			
H_2O-M-His94	114	109	110
H_2O-M-His129	112	111	112
H_2O-M-His292	105	116	111
His94-M-His129	108	104	111
His94-M-His292	105	107	104
His129-M-His292	112	108	109

[a] From the structure of *A. xylosoxidans* WT NIR (determined herein). His300 replaces His292 in the WT protein. [b] From the high-resolution structure of *A. xylosoxidans* WT NIR.

the T1 site, were obtained. Because diffraction data were collected at a wavelength of 1.33 Å, an anomalous difference map was generated to identify the location of any copper in the crystal; the theoretical contribution to the anomalous signal for Cu at 1.33 Å is approximately 3.6 electrons, whereas for Zn it is approximately 0.52 electrons. There were no peaks in this map at either the T2 site or the third metal site (situated between domains and unrelated to the active centre) in the NIRAMI structure, which are both, therefore, assumed to be occupied by Zn^{II}. The only peak in this map is relatively weak (7.4 σ) and is located about 1 Å from the centre of the electron density that dominates the T1 site in the final $2|F_{obs}|-|F_{calcd}|\varphi F_{calcd}$ maps (or $|F_{obs}|-|F_{calcd}|\varphi F_{calcd}$ maps with the metal removed). It would therefore appear that the dominant metal in this site is also Zn^{II}, centred in the electron density. A small amount of Cu^{I} could be present displaced towards the Met, resulting in the slightly ellipsoidal electron density. The most appropriate model that describes the T1-site structure has Zn^{II} bound by His89, Cys130, His133, and a water molecule (Figure 3b and c).

The NIRAMI loop contraction, therefore, has a major influence on the structure of the Zn^{II} T1 centre (Figure 3c and Table 2). The His89 ligand undergoes rotation of its imidazole ring compared with WT NIR, and the thiolate of the coordinating Cys is displaced (Figure 3c). Larger differences were found for the axial Met ligand, with the thioether sulfur displaced about 0.7 Å from its position in WT NIR. The biggest change was observed for the His ligand on the loop, which occupies a totally different position than in WT NIR. This results in the $N^{\delta1}$ atom being much more distant (≈3 Å) from the location of the Cu^{II} ion in WT NIR. The movement of the His residue results in a more open metal centre with increased solvent accessibility, which allows a water molecule to bind to Zn^{II}. The thioether group of Met136 is about 3.6 Å from the metal and is not considered to coordinate. This arrangement results in a highly distorted tetrahedral T1 Zn^{II} site (see Table 2).

The structure of the T2 Zn^{II} site in NIRAMI is almost identical to that of the T2 Cu^{II} site in WT NIR (Figure 3c and Table 3). This metal site has two His ligands (His94 and His129) that are derived from one subunit and one His ligand from an adjacent subunit (all of which coordinate through their $N^{\varepsilon2}$ atoms). The almost perfect tetrahedral coordination geometry is completed by a water ligand that hydrogen bonds with the $O^{\delta2}$ of Asp92.

Discussion

In this study the importance of the extended T1 copper-binding loop in the cupredoxin domain of NIR has been investigated. The variant with a T1 copper-binding loop shortened by over half its length is stable, which allows detailed characterisation. The backbone conformation of the introduced loop in NIRAMI, and the active site hydrogen-bonding pattern, are similar to AMI,[31] although there are larger changes in this region than those observed in the structures of chimeric cupredoxins.[19–21] The isolation of two forms of NIRAMI with slightly different spectroscopic properties suggests that this loop-contraction experiment has introduced flexibility at the Cu^{II} site, a feature that has also been found for other T1 copper site variants.[15,32–35] Both forms of NIRAMI were isolated in monomeric and trimeric forms, which indicates that loop contraction has destabilised the protein's quaternary structure.

The fold of the NIRAMI monomer is very similar to that of WT NIR,[4] so significant changes in the overall structure cannot be responsible for the observed trimer destabilisation. The contact surface areas between monomers, and the properties of this interface, are also alike in the WT NIR and NIRAMI structures. The lowered stability of the NIRAMI trimer observed in solution must therefore be a consequence of localised changes that result from removal and modification of key structural features, which involve the extended loop of WT NIR. These include an α-helical section, various hydrophobic interactions and secondary structure elements adjacent to the ligand-containing loop.

The spectroscopic studies reported herein demonstrate that NIRAMI binds Cu^{II} at the T1 site in an arrangement almost identical to that found in WT NIR. Cu^{II} coordinated in the same geometry as Zn^{II} at the T1 site in the crystal structure of NIRAMI would result in very different spectral features, particularly in the EPR spectra. The T1 site flexibility introduced by the NIRAMI mutation destabilises the Cu^{II} form, which allows displacement by Zn^{II}. The Zn^{II} ion has moved away from Met136 towards the protein surface, and is about 1 Å from the likely location of the small amount of copper detected in the crystal and from the position of the Cu^{II} ion observed when the WT NIR structure is superimposed.[4] The side chain of the His133 ligand in the loop is dramatically displaced compared with the position of the corresponding imidazole in WT NIR;[4] this gives a much more solvent-exposed active site that includes a water ligand. Copper removal and metal substitution at T1 copper centres usually has very little influence on the structure of the active site. For example, Cu^{II},[36–38] Zn^{II},[39] Cd^{II},[40] Ni^{II}[41] Co^{II},[42] and metal-free AZ[43,44] all have metal-site structures that are remarkably alike. Furthermore, the structure of the Met150Glu *Alcaligenes faecalis* NIR variant has a Zn^{II} T1 site at which the arrangement of the three equatorial ligands is very similar to that in the Cu^{II} WT protein.[45] Limited structural change upon metal substitution is one of the most convincing pieces of evidence in favour of a constraining role for the rigid β-barrel domain that always surrounds this particular biological redox site.[24] The T1 site of NIRAMI appears to be flexible and therefore, the extended metal-binding loop in its cupredoxin domain must contribute to constraining this region. Malleability will increase the inner-sphere reorganisation energy of the T1 copper site, which will decrease its ET capabilities (see below).

T1 Cu site differences between the oxidised and reduced forms of NIRAMI affect E_m. Because the major T1 site change between Zn^{II}–NIRAMI and WT Cu^{II}–NIR, involves the coordinating His residue on the loop, protonation and dissociation of this ligand (a feature observed in certain Cu^{I} cupredoxins, including AMI ($pK_a \approx 7$)),[13,27,46,47] is a suitable model of what may occur in NIRAMI upon reduction. Protonation of the His ligand at a T1 site results in Cu^{I} becoming three-coordinate, an arrangement that stabilises this oxidation state of the metal and leads to a striking increase in E_m[13,27,46–49] and a dramatic decrease in ET (owing to an increased reorganisation energy).[50,51] The E_m value for the T1 site of NIRAMI is approximately 200 mV higher than that of WT NIR and agrees with the value reported for the influence of protonation and dissociation of the His ligand on the E_m value of AMI,[47] indicating that structural changes occur in NIRAMI upon reduction to stabilize Cu^{I} over Cu^{II}. The structure of the T2 centre (the site of nitrite binding and reduction) is almost identical in NIRAMI and WT NIR, and its properties, including the E_m value, should not have been significantly influenced by the loop contraction. The dramatic effect of the NIRAMI mutation on activity is therefore partly due to it no longer being thermodynamically favourable for ET to occur from the T1 to the T2 site as a result of the increased E_m value of the T1 copper site. A similar effect has been seen in other T1 site mutants of NIR that raise the E_m value.[30,52–54] An increased reorganisation energy of the T1 site will also inhibit ET between the two copper sites of the enzyme, as suggested for variants of NIR[52,55] and cupredoxins,[56,57] and must also contribute to the decreased catalytic activity of NIRAMI.

Conclusion

The replacement of the longest T1 copper-binding loop in the multi-copper, multi-domain enzyme NIR with the shortest known naturally occurring sequence for this class of ubiquitous ET site has a significant effect on structure and activity. The T1 site is flexible in the NIRAMI loop variant and the native metal is readily replaced by Zn^{II}, which gives an arrangement different to that found for Cu^{II}. This is an unusual observation for a T1 copper site, in which the constrained environment usually imposes the same geometry on a range of non-native metals. Structural changes at this site must also occur upon reduction of copper, which gives rise to the large increase in E_m for this site compared with WT NIR. Efficient ET to the structurally unaltered substrate-binding T2 site is dramatically decreased due to an unfavourable driving force and an increased reorganisation energy for the T1 site. The extended loop in NIR is important for simultaneously stabilising a functional T1 copper site and the trimeric arrangement of this enzyme.

Experimental Section

Mutagenesis: Loop mutagenesis was carried out by using QuikChange (Stratagene) site-directed mutagenesis. A pGEMT derivative (pGEMT bNIR) was used as the template that harboured the gene for *A. xylosoxidans* NCIMB11015 NIR.[58] The primers used to mutate the C^{130}APEGMVPWH^{139}VVSGM^{144} (T1 copper ligands numbered) loop of *A. xylosoxidans* WT NIR to C^{130}TPH^{133}PFM^{136}, which is the sequence of the corresponding loop in AMI from both *P. versutus* and *P. denitrificans*, were gcaccttcgtctaccactgcaccccgcacccgtttatgagcggcacgctg (forward) and cagcgtgccgctcataaacgggtgcggggtgcagtggtagacgaaggtgc (reverse). Both strands of the mutated plasmid pGEMT-bNIRAMI were sequenced and the *NdeI* and *XhoI* insert was re-cloned into pET22b (Novagene) to give pET22b-bNIRAMI.

Overexpression and purification of WT NIR and NIRAMI: *Escherichia coli* BL21 was transformed by using either pET22b-bNIR (WT NIR) or

pET22b-bNIRAMI, cells were grown and the WT protein was isolated as previously described.[58] In the case of NIRAMI, the cell pellet from 8 L of culture was re-suspended in a 20 mM solution of 2-(*N*-morpholino)-ethanesulphonic acid (Mes, pH 6.0; Sigma), disrupted by sonication, and centrifuged. Aliquots of a 0.5 M solution of $CuSO_4$ were added to the supernatant (final concentration 1.5 mM), which was incubated overnight at 4 °C. The solution was then centrifuged and the supernatant was loaded onto an SP sepharose (GE Healthcare) column equilibrated with 20 mM Mes (pH 6.0). The bound proteins were eluted with a pH gradient by using equal volumes of 20 mM Mes (pH 6.0) and 50 mM tris(hydroxymethyl)aminomethane (Tris; pH 9.5). The NIRAMI fractions were combined and exchanged into 10 mM Tris (pH 9.5), then loaded onto a Hi-Trap Q HP column (GE Healthcare) equilibrated with the same buffer and eluted with 25 mM phosphate (pH 6.0). The NIRAMI-containing fractions were pooled and exchanged into a solution of 20 mM Tris (pH 8.0) and 200 mM NaCl by using ultrafiltration. The final purification step was carried out on a Superdex 200 (GE Healthcare) gel filtration column that had been equilibrated with the same buffer. This column was calibrated by using low and high molecular weight kits (GE Healthcare). Pure NIRAMI has an $A_{280}/A_{\approx 600}$ ratio of around 12 for the fully oxidised enzyme and purity was verified by using sodium dodecyl sulfate–polyacrylamide gel electrophoresis (12.5 % gel). The absorbance ratio increases with time and could not be fully restored by oxidation, which is indicative of copper loss. Protein concentrations were determined by using the ε values of the main blue bands ($\varepsilon = 4400$ and $5200\ M^{-1}cm^{-1}$ for NIRAMI and WT NIR, respectively; see below). These differences in the ε values are consistent with the higher $A_{280}/A_{\approx 600}$ ratio usually obtained for NIRAMI than WT NIR (≈ 11).

UV/Vis spectroscopy: Determination of ε and molecular weight: All UV/Vis spectra were acquired at 25 °C by using a Perkin–Elmer λ 35 spectrophotometer. To determine the ε values, copper concentrations were measured by using an M Series atomic absorption spectrophotometer (Thermo Electron) with standards in the range of 0.2 to 1.8 ppm Cu^{II} made from a stock solution (Aldrich). The protein was fully oxidised with a solution of $K_3[Fe(CN)_6]$, washed with 0.5 mM ethylenediaminetetraacetic acid (EDTA) and exchanged into 2 mM Tris (pH 8.6) by using ultrafiltration. A UV/Vis spectrum was obtained and the copper concentration of the same sample determined. Molecular weights were determined by MALDI-TOF mass spectrometry.

Sample preparation and EPR spectroscopy: X-band EPR spectra were recorded at −196 °C by using a Bruker EMX spectrometer. Diphenylpicrylhydrazyl (DPPH) was used as an external reference, and the SIMFONIA program (Bruker) was used for spectral simulations. The samples were washed with 0.5 mM EDTA and fully oxidised with excess $K_3[Fe(CN)_6]$, then the EDTA was removed by using ultrafiltration with 25 mM *N*-(2-hydroxyethyl)piperazine-*N*′-(2-ethanesulfonic acid) (Hepes, pH 8.6) or 20 mM Tris (pH 7.5).

Electrochemistry: The direct measurement of E_m values was carried out by using cyclic voltammetry at ambient temperature ((23 ± 1) °C) with an electrochemical setup described previously.[59] The gold working electrode was polished with a slurry of Al_2O_3 (particle size = 0.015 μm, BDH) on fresh Buehler cloth. After polishing, the electrode was sonicated for 10 min and then modified by immersion in a saturated solution of 3,3′-dithiodipropionic acid for 25 min. Cyclic voltammograms could only be obtained for $NIRAMI_{600}$ (a reproducible electrochemical response could not be achieved for $NIRAMI_{610}$).

Nitrite reductase activity assay: The activities of WT NIR and trimeric $NIRAMI_{610}$ were compared by measuring the rate of oxidation of dithionite-reduced MV.[28,29] Samples were incubated with an excess of Cu^{II} for about 2 weeks at 4 °C to ensure high T2 Cu site occupancy. The reaction mixture (1 mL) contained 50 mM phosphate (pH 7.0), 80 μM MV, 0.1–10 mM KNO_2 and 2 mM sodium dithionite. The reaction was initiated by the addition of 2 μL of enzyme solution (1 μM for both WT NIR and NIRAMI in 50 mM phosphate; pH 7.0), and the absorbance decrease at 600 nm ($\varepsilon_{600} = 12\ mM^{-1}cm^{-1}$) due to the oxidation of MV was monitored. A blank reaction was also carried out by using buffer (2 μL) instead of enzyme solution and was subtracted as a baseline. Relative activity was obtained from comparisons of the rate of absorbance decrease at 600 nm at identical nitrite concentrations. The absorbance changes in the case of NIRAMI were so small that they were difficult to determine precisely, except at the highest nitrite concentration, which demonstrated that NIRAMI is almost totally inactive and made detailed analysis of these data difficult.

Crystallisation and structure analysis: Numerous attempts to crystallise both Cu^{II}–$NIRAMI_{600}$ and Cu^{II}–$NIRAMI_{610}$ were undertaken by using the hanging drop method of vapour diffusion at 20 °C. This included the use of commercially available solutions, such as the PACT and Structure 1 and 2 screens (Molecular Dimensions, UK), which included diluted versions with protein concentrations that ranged from 2 to 10 $mg\,mL^{-1}$. Furthermore, crystallisation trials were undertaken by using buffer/precipitant combinations that had previously proven successful for WT and mutants of *A. xylosoxidans* NIR.[4,30,52,60] The best crystal was obtained with the trimeric form of Cu^{II}–$NIRAMI_{610}$ by using a solution of protein (2.0 μL, 2.5 $mg\,mL^{-1}$) in Tris (5 mM, pH 8.6) mixed with a precipitant solution (2.0 μL) containing 50 mM Hepes pH 7.0, 5 mM $ZnCl_2$ and 10 % polyethylene glycol (PEG) 6000. This crystal took a few months to form and was completely colourless. Prior to being frozen in a stream of nitrogen, the crystal was immersed in N-paratone oil as a cryo-protectant. Crystals of Cu^{II} *A. xylosoxidans* WT NIR were obtained by using the hanging drop vapour diffusion method at 20 °C with a solution of protein (1.5 μL, 10 $mg\,mL^{-1}$) in 5 mM Tris (pH 8.6) mixed with precipitant solution (1.5 μL) containing 100 mM Mes pH 6.5, 10 mM $ZnSO_4{\cdot}7H_2O$ and 25 % PEG-MME 550 (MME = monomethyl ether). Crystals formed overnight and were bright blue. Prior to being frozen in a stream of nitrogen, a crystal was immersed in 10 % glycerol, 100 mM Mes pH 6.5, 10 mM $ZnSO_4{\cdot}7H_2O$ and 28 % PEG-MME 550 as a cryo-protectant. Diffraction data for NIRAMI were collected at 100 K at the Daresbury synchrotron radiation source (station 10.1 operating at 1.33 Å) by using a MAR225 CCD detector. This wavelength was chosen to maximize the anomalous scattering contribution of copper and enable the position of this metal to be determined in the model by using anomalous difference maps. Owing to deterioration of the crystal in the X-ray beam, only 57° of data were collectable. Diffraction data for WT NIR were collected at 93 K on a Rigaku Raxis IV^{++} detector with X-rays from a Micromax-007 generator fitted with Osmic "blue" optics. All data were processed with MOSFLM[61] and scaled with SCALA.[62] R_{free} was calculated by using 5 % of the data that had been set aside. The structures were solved by

Table 4. Crystallographic data collection and refinement statistics.

	WT NIR	NIRAMI
data collection[a]		
λ [Å]	1.542	1.330
space group	*H*3	*H*3
resolution range [Å]	34.14–2.35 (2.48–2.35)	37.53–2.50 (2.64–2.50)
unit cell parameters [Å]	$a = b = 89.45$ $c = 144.47$	a = b = 89.81 c = 143.10
no. of unique reflections	17939 (2599)	14625 (2183)
redundancy	5.4 (5.3)	1.8 (1.8)
$I/\sigma(I)$	25.9 (4.6)	10.4 (2.7)
completeness [%]	100 (100)	98.4 (99.9)
R_{merge} [%]	5.3 (31.5)	5.6 (27.5)
refinement[a]		
resolution range [Å]	34.14–2.35 (2.41–2.35)	37.53–2.50 (2.57–2.50)
R_{factor} [%]	16.5 (19.9)	18.1 (24.7)
R_{free} [%]	21.5 (33.2)	23.2 (30.7)
RMSD bond lengths [Å]	0.013	0.013
RMSD bond angles [°]	1.54	1.54
average *B*-factor (protein) [Å^2]	39.1	54.8
average B-factor (ligand) [Å^2]	42.7	55.8
ramachandran outliers [%]	1.4	1.4

[a] Figures in parentheses represent data for the highest resolution shell.

using molecular replacement with MOLREP (implemented in CCP4)[62] and the high-resolution (1.04 Å) structure for WT NIR[4] (PDB entry 1OE1, with the C-terminal ligand-containing loop, copper atoms, and water molecules removed) was used as a search model. Iterative model building (by using COOT)[63] and refinement (REFMAC5)[64] cycles were used to complete the structures. Detailed data collection, processing, and refinement statistics are given in Table 4. Ramachandran outliers were identified by using MOLEMAN2,[65] whereas LSQMAN[66] was used to generate all superimposed structures and determine RMSDs for C^{α} atoms, except for the AMI/NIRAMI comparison, which used the Secondary Structure Motif (SSM) algorithms implemented in COOT. Surface area calculations were performed by using PISA on the EBI website (http://www.ebi.ac.uk/msd-srv/prot_int/pistart.html)[67] and by using the Protein–Protein Interaction Server.[68] Figures of protein structures were prepared with Pymol.[69] The coordinates and structure factors for NIRAMI and WT NIR have been deposited with the Protein Data Bank, and have the PDB ID codes 2vmj and 2vn3.

Acknowledgements

We thank the BBSRC (grant number BB/C504519) and Newcastle University for funding, and the staff of the Daresbury synchrotron radiation source for assistance with data collection (especially Mark J. Ellis). M.J.B. is supported by a Royal Society (UK) University Research Fellowship.

[1] S. Suzuki, K. Kataoka, K. Yamaguchi, *Acc. Chem. Res.* **2000**, *33*, 728–735.
[2] E. T. Adman, J. W. Godden, S. Turley, *J. Biol. Chem.* **1995**, *270*, 27458–27474.
[3] F. E. Dodd, J. Van Beeumen, R. R. Eady, S. S. Hasnain, *J. Mol. Biol.* **1998**, *282*, 369–382.
[4] M. J. Ellis, F. E. Dodd, G. Sawers, R. R. Eady, S. S. Hasnain, *J. Mol. Biol.* **2003**, *328*, 429–438.
[5] S. V. Antonyuk, R. W. Strange, G. Sawers, R. R. Eady, S. S. Hasnain, *Proc. Natl. Acad. Sci. USA* **2005**, *102*, 12041–12046.
[6] M. Nojiri, Y. Xie, T. Inoue, T. Yamamoto, H. Matsumura, K. Kataoka, Deligeer, K. Yamaguchi, Y. Kai, S. Suzuki, *Proc. Natl. Acad. Sci. USA* **2007**, *104*, 4315–4320.
[7] E. T. Adman, *Adv. Protein Chem.* **1991**, *42*, 145–197.
[8] M. E. P. Murphy, P. F. Lindley, E. T. Adman, *Protein Sci.* **1997**, *6*, 761–770.
[9] A. Impagliazzo, L. Krippahl, M. Ubbink, *ChemBioChem* **2005**, *6*, 1648–1653.
[10] C. Dennison, *Dalton Trans.* **2005**, 3436–3442.
[11] C. Dennison, *Coord. Chem. Rev.* **2005**, *249*, 3025–3054.
[12] C. Dennison, *Nat. Prod. Rep.* **2008**, *25*, 15–24.
[13] C. Dennison, E. Vijgenboom, W. R. Hagen, G. W. Canters, *J. Am. Chem. Soc.* **1996**, *118*, 7406–7407.
[14] R. Remenyi, L. J. C. Jeuken, P. Comba, G. W. Canters, *J. Biol. Inorg. Chem.* **2001**, *6*, 23–26.
[15] C. Buning, G. W. Canters, P. Comba, C. Dennison, L. Jeuken, M. Melter, J. Sanders-Loehr, *J. Am. Chem. Soc.* **2000**, *122*, 204–211.
[16] S. Yanagisawa, C. Dennison, *J. Am. Chem. Soc.* **2003**, *125*, 4974–4975.
[17] S. Yanagisawa, C. Dennison, *J. Am. Chem. Soc.* **2004**, *126*, 15711–15719.
[18] G. Battistuzzi, M. Borsari, G. W. Canters, G. di Rocco, E. de Waal, Y. Arendsen, A. Leonardi, A. Ranieri, M. Sola, *Biochemistry* **2005**, *44*, 9944–9949.
[19] C. Li, S. Yanagisawa, B. M. Martins, A. Messerschmidt, M. J. Banfield, C. Dennison, *Proc. Natl. Acad. Sci. USA* **2006**, *103*, 7258–7263.
[20] C. Li, M. J. Banfield, C. Dennison, *J. Am. Chem. Soc.* **2007**, *129*, 709–718.
[21] M. Velarde, R. Huber, S. Yanagisawa, C. Dennison, A. Messerschmidt, *Biochemistry* **2007**, *46*, 9981–9991.
[22] B. G. Malmström, *Eur. J. Biochem.* **1994**, *223*, 711–718.
[23] R. J. P. Williams, *Eur. J. Biochem.* **1995**, *234*, 363–381.
[24] H. B. Gray, B. G. Malmström, R. J. P. Williams, *J. Biol. Inorg. Chem.* **2000**, *5*, 551–559.
[25] U. Ryde, M. H. M. Olsson, K. Pierloot, B. O. Roos, *J. Mol. Biol.* **1996**, *261*, 586–596.
[26] T. Kohzuma, S. Shidara, K. Yamaguchi, N. Nakamura, Deligeer, S. Suzuki, *Chem. Lett.* **1993**, 2029–2032.
[27] G. Battistuzzi, M. Borsari, G. W. Canters, E. de Waal, A. Leonardi, A. Ranieri, M. Sola, *Biochemistry* **2002**, *41*, 14293–14298.
[28] T. Kakutani, H. Watanabe, K. Arima, T. Beppu, *J. Biochem.* **1981**, *89*, 453–461.
[29] Z. H. L. Abraham, D. J. Lowe, B. E. Smith, *Biochem. J.* **1993**, *295*, 587–593.
[30] M. A. Hough, M. J. Ellis, S. Antonyuk, R. W. Strange, G. Sawers, R. R. Eady, S. S. Hasnain, *J. Mol. Biol.* **2005**, *350*, 300–309.
[31] L. M. Cunane, Z. W. Chen, R. C. E. Durley, F. S. Mathews, *Acta Crystallogr. Sect. D* **1996**, *52*, 676–686.
[32] T. den Blaauwen, G. W. Canters, *J. Am. Chem. Soc.* **1993**, *115*, 1121–1129.
[33] G. van Pouderoyen, C. R. Andrew, T. M. Loehr, J. Sanders-Loehr, S. Mazumdar, H. A. O. Hill, G. W. Canters, *Biochemistry* **1996**, *35*, 1397–1407.
[34] B. G. Karlsson, L. C. Tsai, H. Nar, J. Sanders-Loehr, N. Bonander, V. Langer, L. Sjölin, *Biochemistry* **1997**, *36*, 4089–4095.
[35] A. Messerschmidt, L. Prade, S. J. Kroes, J. Sanders-Loehr, R. Huber, G. W. Canters, *Proc. Natl. Acad. Sci. USA* **1998**, *95*, 3443–3448.
[36] E. N. Baker, *J. Mol. Biol.* **1988**, *203*, 1071–1095.
[37] H. Nar, A. Messerschmidt, R. Huber, M. van de Kamp, G. W. Canters, *J. Mol. Biol.* **1991**, *221*, 765–772.
[38] B. R. Crane, A. J. Di Bilio, J. R. Winkler, H. B. Gray, *J. Am. Chem. Soc.* **2001**, *123*, 11623–11631.
[39] H. Nar, R. Huber, A. Messerschmidt, A. C. Filippou, M. Barth, M. Jaquinod, M. van de Kamp, G. W. Canters, *Eur. J. Biochem.* **1992**, *205*, 1123–1129.
[40] K. A. Blackwell, B. F. Anderson, E. N. Baker, *Acta Crystallogr. Sect. D* **1994**, *50*, 263–270.
[41] J. M. Moratal, A. Romero, J. Salgado, A. Perales-Alarcón, H. R. Jiménez, *Eur. J. Biochem.* **1995**, *228*, 653–657.
[42] N. Bonander, T. Vänngård, L. C. Tsai, V. Langer, H. Nar, L. Sjölin, *Proteins: Struct. Funct. Bioinf.* **1997**, *27*, 385–394.
[43] H. Nar, A. Messerschmidt, R. Huber, M. Van de Kamp, G. W. Canters, *FEBS Lett.* **1992**, *306*, 119–124.
[44] W. E. B. Shepard, R. L. Kingston, B. F. Anderson, E. N. Baker, *Acta Crystallogr. Sect. D* **1993**, *49*, 331–343.
[45] M. E. P. Murphy, S. Turley, M. Kukimoto, M. Nishiyama, S. Horinouchi, H. Sasaki, M. Tanokura, E. T. Adman, *Biochemistry* **1995**, *34*, 12107–12117.
[46] Z. Zhu, L. M. Cunane, Z. W. Chen, R. C. E. Durley, F. S. Mathews, V. L. Davidson, *Biochemistry* **1998**, *37*, 17128–17136.
[47] L. J. C. Jeuken, R. Camba, F. A. Armstrong, G. W. Canters, *J. Biol. Inorg. Chem.* **2002**, *7*, 94–100.
[48] J. M. Guss, P. R. Harrowell, M. Murata, V. A. Norris, H. C. Freeman, *J. Mol. Biol.* **1986**, *192*, 361–387.
[49] F. A. Armstrong, H. A. O. Hill, B. N. Oliver, D. Whitford, *J. Am. Chem. Soc.* **1985**, *107*, 1473–1476.
[50] A. J. Di Bilio, C. Dennison, H. B. Gray, B. E. Ramirez, A. G. Sykes, J. R. Winkler, *J. Am. Chem. Soc.* **1998**, *120*, 7551–7556.
[51] K. Sato, T. Kohzuma, C. Dennison *J. Am. Chem. Soc.* **2003**, *125*, 2101–2112.
[52] M. J. Ellis, M. Prudêncio, F. E. Dodd, R. W. Strange, G. Sawers, R. R. Eady, S. S. Hasnain, *J. Mol. Biol.* **2002**, *316*, 51–64.
[53] M. Prudêncio, G. Sawers, S. A. Fairhurst, F. K. Yousafzai, R. R. Eady, *Biochemistry* **2002**, *41*, 3430–3438.
[54] H. J. Wijma, M. J. Boulanger, A. Molon, M. Fittipaldi, M. Huber, M. E. P. Murphy, M. P. Verbeet, G. W. Canters, *Biochemistry* **2003**, *42*, 4075–4083.

[55] H. J. Wijma, I. MacPherson, O. Farver, E. I. Tocheva, I. Pecht, M. P. Verbeet, M. E. P. Murphy, G. W. Canters, *J. Am. Chem. Soc.* **2007**, *129*, 519–525.
[56] M. D. Harrison, C. Dennison, *ChemBioChem* **2004**, *5*, 1579–1581.
[57] S. Yanagisawa, C. Dennison, *J. Am. Chem. Soc.* **2005**, *127*, 16453–16459.
[58] K. Sato, C. Dennison, *Chem. Eur. J.* **2006**, *12*, 6647–6659.
[59] C. Dennison, A. T. Lawler, T. Kohzuma, *Biochemistry* **2002**, *41*, 552–560.
[60] M. J. Ellis, S. Antonyuk, S. S. Hasnain, *Acta Crystallogr. Sect. D* **2002**, *58*, 456–458.
[61] A. Leslie, *Joint CCP4 + ESF-EAMCB Newsletter on Protein Crystallography*, **1992**, No. 26.
[62] Collaborative Computational Project, Number 4 (CCP4), *Acta Crystallogr. Sect. D* **1994**, *50*, 760–763.
[63] P. Emsley, K. Cowtan, *Acta Crystallogr. Sect. D* **2004**, *60*, 2126–2132.
[64] G. N. Murshudov, A. A. Vagin, E. J. Dodson, *Acta Crystallogr. Sect. D* **1997**, *53*, 240–255.
[65] G. J. Kleywegt, T. A. Jones, *Structure* **1996**, *4*, 1395–1400.
[66] G. J. Kleywegt, J. Y. Zou, M. Kjeldgaard, T. A. Jones in *International Tables for Crystallography, Vol. F: Crystallography of Biological Macromolecules* (Eds.: M. G. Rossmann, E. Arnold), **2001**, pp. 353–356, 366–367, Kluwer Academic, Dordrecht.
[67] E. Krissinel, K. Henrick in *Lecture Notes in Computer Science, Vol. 3695: Computational Life Sciences*, (Eds.: M. R. Berthold, R. Glen, K. Diederichs, O. Kohlbacher, I. Fischer), Springer, Berlin, **2005**, pp. 163–174.
[68] S. Jones, J. M. Thornton, *Proc. Natl. Acad. Sci. USA* **1996**, *93*, 13–20.
[69] W. L. DeLano, The PyMOL Molecular Graphics System, DeLano Scientific, Palo Alto, CA, USA, **2002**.
[70] M. J. Ellis, personal communication

Received: December 18, 2007
Published online: May 19, 2008

